

EgoCampus: Egocentric Pedestrian Eye Gaze Model and Dataset

Ronan John[†]

Aditya Kesari[†]

Vincenzo DiMatteo[†]

Kristin Dana

Rutgers University, New Brunswick

ronan.john, aditya.kesari, vincenzo.dimatteo, kristin.dana@rutgers.edu

Abstract

We address the challenge of predicting human visual attention during real-world navigation by measuring and modeling egocentric pedestrian eye gaze in an outdoor campus setting. We introduce the **EgoCampus** dataset, which spans 25 unique outdoor paths over 6 km across a university campus with recordings from more than 80 distinct human pedestrians, resulting in a diverse set of gaze-annotated videos. The system used for collection, Meta’s Project Aria glasses, integrates eye tracking, front-facing RGB cameras, inertial sensors, and GPS to provide rich data from the human perspective. Unlike many prior egocentric datasets that focus on indoor tasks or exclude eye gaze information, our work emphasizes visual attention while subjects walk in outdoor campus paths. Using this data, we develop **EgoCampusNet**, a novel method to predict eye gaze of navigating pedestrians as they move through outdoor environments. Our contributions provide both a new resource for studying real-world attention and a resource for future work in gaze prediction models for navigation. Dataset and code are available upon request, and will be made publicly available at a later date at <https://github.com/ComputerVisionRutgers/EgoCampus>

1. Introduction

Understanding where humans look as they navigate the world is fundamental for interpreting behavior and intent. Gaze patterns reveal common fixations, saccades, and attention shifts, offering insight into how people prioritize visual information in complex environments. Understanding human gaze and visual attention is particularly relevant for training embodied agents operating in shared human spaces, where prediction models may support navigation, cooperation, or anticipatory behavior. Much of the prior research in eye gaze has focused on constrained tasks or environments,

[†]Denotes equal contribution

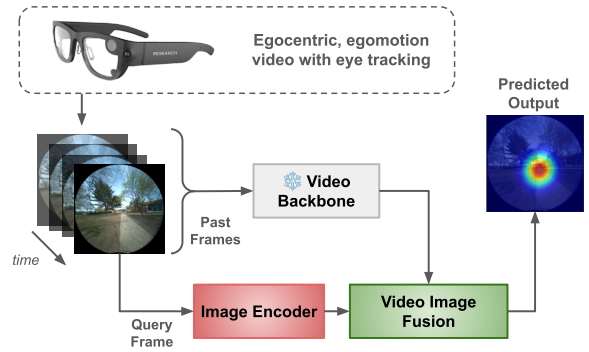


Figure 1. **Overview of our proposed gaze prediction model, ECN.** The Project Aria glasses capture a stream of egocentric video. From this video, we extract features with a pretrained backbone. From the query image (usually the last frame), we extract features with a trained image encoder. Lastly, the video and image features are fused and decoded in order to predict the final output, representing where people are most likely to look during egocentric motion.

such as gaze on static images, screen-based videos, structured indoor activities like cooking, cleaning, and carpentry. The recent large-scale egocentric dataset Ego4D [12] is a pioneering dataset with large variation of subjects, tasks and context. While Ego4D primarily consists of egocentric videos of tasks, eye gaze was captured on a small subset and the focus is not outdoor pedestrian locomotion.

Research on eye gaze in outdoor environments during navigation is still in its early stages.

In this work, we introduce: (1) EgoCampus, a pedestrian egocentric dataset capturing synchronized eye gaze, video, and sensor data as participants navigate real-world outdoor routes on a university campus; and (2) EgoCampusNet (ECN) (Fig. 1), a prediction model leveraging a pre-trained video backbone and an eye gaze predictor head. EgoCampus is tightly focused on eye gaze of pedestrians walking outdoors in a campus setting, and it comprises multiple

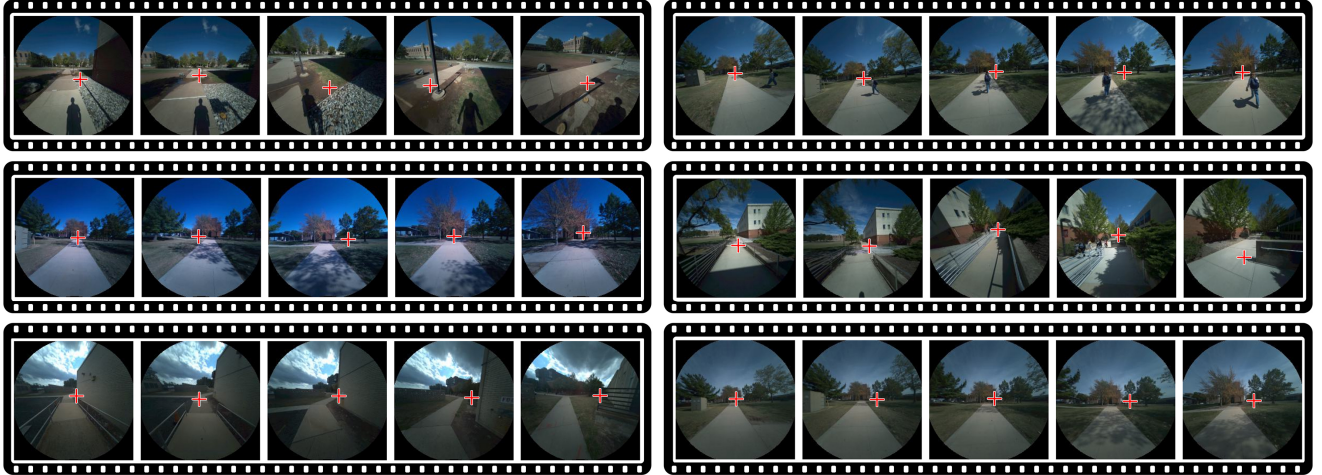


Figure 2. **Samples of video sequences from the EgoCampus dataset.** EgoCampus contains 32 hours of video from the Project Aria glasses, capturing egocentric video from 82 pedestrians traversing 25 distinct paths on a university campus. Each frame has an associated eye gaze coordinate (shown above as the red “+”) and auxiliary sensor readings (IMU, GPS, Wi-Fi).

subjects traveling similar routes. This framework enables both individual analysis and cross-subject comparisons of gaze behavior across shared spatio-temporal contexts. All data is collected using Meta’s Project Aria glasses [7], providing high-resolution RGB video, gaze coordinates, inertial measurements, and GPS. This combination allows us to model and analyze pedestrian eye gaze during locomotion over a range of subjects. Our EgoCampus dataset spans 25 unique outdoor paths over 6 km across a university campus with recordings from more than 80 distinct human pedestrians (see Fig. 2). The entire dataset will be made publicly available and provides a valuable resource for understanding pedestrian spatial attention, with strong potential for navigation applications such as developing spatio-temporal environment-sampling methods that mimic human attention.

To summarize, our contributions are as follows:

- An egocentric video dataset (with eye gaze) collected during pedestrian locomotion. (EgoCampus)
- A novel model for efficiently learning to predict gaze from egocentric video. (EgoCampusNet)
- An evaluation of model performance using the EgoCampus dataset and ECN including an ablation study over video feature backbones.

2. Related Work

Gaze Prediction. As a person moves through their environment, their attention is often split between objects that are visually salient and objects that provide task-relevant information [5, 48]. Gaze prediction requires task-specific dependencies to be captured in order to accurately predict fixations. Li et al. [28] sought to predict eye gaze in egocentric

video, modeling the temporal dynamics of gaze for object segmentation and action recognition. They advanced this research by combining head motion in gaze prediction in egocentric settings. Seminal work [8] established that gaze and actions are mutually informative in egocentric video in the context of recognition. The scope was expanded beyond “where people look” to “when they stop looking”, modeling human attention dynamics even when visual goals are not present [51]. Park et al. [40] modeled saliency in social settings, encoding the relative positions of people in a scene to capture task-specific interaction. Work from Thakur et al. [41] also predicted gaze in a social setting, but incorporated IMU readings from the capture device. More modern work [3, 27, 32] integrates transformers and diffusion models for efficient goal-directed gaze prediction.

Saliency Prediction. Saliency maps offer a compact, interpretable representation of where attention concentrates, making them well suited for modeling egocentric video data. Early computational models, such as the Itti-Koch multi-scale feature integration approach [16], established the principle that visual contrasts drive attention. Graph-Based Visual Saliency (GBVS) [13] further demonstrated how global graph normalization yields robust saliency. With deep learning, Convolutional Neural Networks (CNNs) dramatically improved prediction quality: Huang et al. [15] introduced a dual-stream CNN capturing coarse and fine features, and Jia et al. [17] proposed EML-Net, an ensemble of pretrained backbones fused through multi-layer decoding. Transformer architectures now dominate the field by modeling long-range spatial and temporal dependencies. SUM [14] unifies image and video saliency with Mamba blocks, while recent works

[25, 27] leverage token-level attention across frames. Other recent advances include models that use pretrained backbones to assist in predicting saliency [26, 30], models that leverage saliency over time [1, 11], and new saliency challenges [33]. A key line of research directly compares predicted saliency with recorded gaze, showing saliency maps correlate with human fixations in egocentric video [50]. However, most evaluations remain confined to static images or short clips. We compare saliency and measured eye gaze by aggregating gaze across continuous outdoor traversals (after aligning frames). In this manner, we introduce a new setting for assessing how modern saliency models align with true spatial attention during navigation, advancing beyond isolated frame-level benchmarks to cumulative, environment-aware attention modeling in the wild.

Egocentric and Gaze Prediction Datasets. Egocentric datasets study how individuals interact with the world by recording first-person viewpoint video from an egocentric camera. Studying eye movements to record gaze was a complex task in the past, with in-lab apparatus required [23]. Traditionally, eye gaze datasets were obtained with human subjects in a lab looking at a screen observing either static images or video. Examples of static-image studies include MIT1003 [19], that uses eye-tracking to measure free-viewing saliency on desktop displays; SALICON [18], which uses mouse movement as a proxy for eye-tracking to record saliency and scales via crowdsourced annotations; and Coco-search18 [4], which has eye gaze from 10 people searching for each of 18 target-object categories in 6000+ natural-scene images. In video-based studies, the subject is fixed and watching pre-recorded actions [36, 44, 45]. In another paradigm called third-person gaze, the subjects are people depicted in static pre-captured images, and their static eye gaze direction in screen coordinates is estimated [20, 39]. Prior paradigms with fixed scenes and static subjects are quite different from our EgoCampus scenario, where pedestrians walk and navigate in the real world.

Advances in eye-tracking algorithms [24] paved the way for wearable headsets and glasses for mobile, in-the-wild eye gaze datasets. Similarly, the ubiquity of head-mounted cameras (e.g. GoPro) support egocentric datasets without eye gaze. Many of the recent datasets emphasize task completion in structured indoor scenes, such as EPIC-Kitchens [6], HD-EPIC [37], HoloAssist [46], and EGTEA Gaze+ [29], which provide gaze-annotated video for action recognition, primarily in kitchen environments. These datasets are not directly relevant to outdoor navigation. Recent work on large-scale egocentric videos like Ego4D [12] have limited eye-gaze measurements, especially for outdoor navigation. The GEETUP [43] dataset is more closely related to our work. This dataset depicts subjects navigating two paths utilizing the Tobii PRO Glasses 2 wearable eye trackers.

The dataset provides RGB images, segmentation and depth maps with 43 subjects on two non-overlapping paths. Our dataset offers several advantages over GEETUP. GEETUP’s clips are segmented due to instances such as subjects pausing to talk or check phones, resulting in a median clip length of 14.7 seconds. In contrast, EgoCampus contains continuous path trajectories averaging 108.2 seconds per clip. EgoCampus also includes over twice as many subjects (82 pedestrians) and paths are traversed in both directions (forward and reverse). Additionally, the use of Project Aria glasses [7] enables the capture of rich auxiliary data, in addition to egocentric eye gaze and video, including IMUs, barometer, magnetometer, GPS, and Wi-Fi/Bluetooth signals. After release of eye tracking glasses from Project Aria, there have been recent expansions in egocentric datasets in varied environments [22, 34, 35, 47]. Aria Navigation Dataset (AND) [34] explores outdoor egomotion and develops a model for head pose, but the dataset seems to have few subjects (an exact count is not provided in the paper). As shown in Tab. 1 our EgoCampus dataset fills a gap in the current work, providing consistent egocentric RGB video and gaze recordings (augmented with IMU, GPS, Wi-Fi) across a large number of participants traversing identical outdoor campus routes, enabling cross-subject comparison in real-world navigation contexts.

3. Dataset

3.1. Dataset Collection

Hardware. Our data collection hardware is the Project Aria glasses, a lightweight, non-intrusive device designed for egocentric research [7]. We captured data from its sensor suite, including a front-facing RGB camera (1408×1408 resolution at 30Hz) and two monochrome, global-shutter, inward-facing cameras for eye tracking. Motion and localization data were simultaneously recorded from the integrated inertial measurement units (IMUs), magnetometer, barometer, Wi-Fi and Bluetooth transceiver, and GPS. This combination of high-resolution video, gaze tracking, and motion sensors provides a rich, multimodal data stream from the human perspective.

Recording protocol. The dataset was collected from 82 unique subjects navigating 25 predefined paths on Busch Campus at Rutgers University. Paths ranged in length from as short as 100 meters to as long as 200 meters with an average length of 150 meters. Data collection followed a structured protocol where each subject was instructed to walk several of these paths individually. Before starting a trajectory, participants were given a bird’s-eye view map showing the start and end points, an example of which is shown in Fig. 3. To ensure a robust capture of real-world variability, recordings spanned different times of the day, multiple seasons, and various weather conditions, yielding

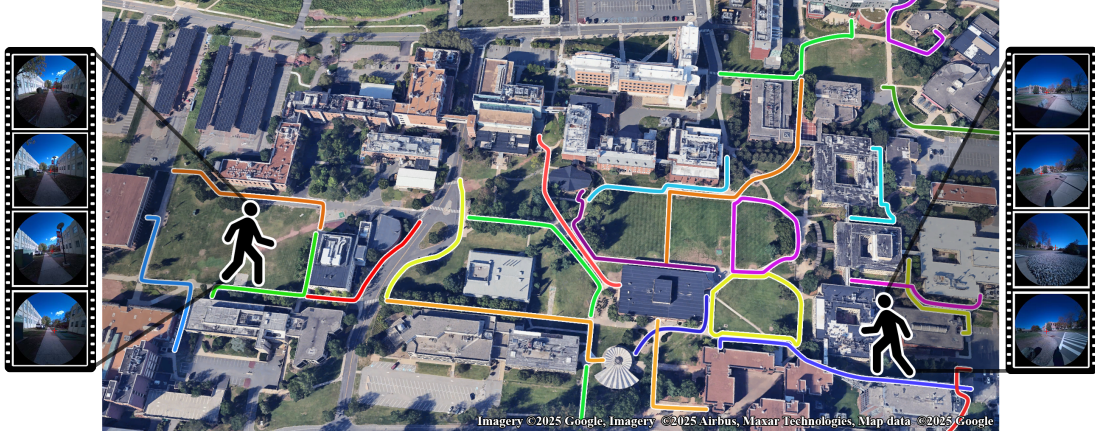


Figure 3. **Dataset Paths.** A map showing a subset of the campus region, with colored paths indicating the participants’ walking trajectories. During data collection, each participant follows a set of paths forwards and backwards. A sample of the captured egocentric video is shown.

a diverse set of environmental conditions.

Data Processing. To prepare the dataset, we performed a multi-stage processing pipeline. First, the raw VRS files were utilized to calculate the eye tracking metrics. Per an internal review board (IRB) policy and agreements with Meta, VRS files are then modified to blur passerby in the video who did not consent to be in the dataset using EgoBlur [38]. We extracted and temporally aligned the raw VRS recordings with multimodal sensor streams. The 1408×1408 30Hz RGB video was downsampled and saved as 224×224 pixel JPEG frames. Both the raw and downsampled video are included in our release of the dataset. Some of the sensor readings, such as the IMU, occurred at a higher frequency than the RGB camera. To create synchronized ground truth, the 30Hz eye-tracking coordinates were saved to a NumPy array with each entry corresponding to the nearest timestamped RGB frame. The high-frequency (1000Hz) IMU readings were aligned by averaging all sensor data (accelerometer, gyroscope) that occurred closest in time to each frame’s timestamp and storing the result in a parallel NumPy file. This processed format facilitates efficient data loading by allowing researchers to directly index a frame and its corresponding gaze and motion data. When using data for training and inference, a set of frames constituting a video clip is sampled at a fixed interval, in a sliding window fashion.

Privacy and Ethics. All data collection procedures were designed to be privacy-preserving and adhered to a strict IRB protocol for human subjects research. In accordance with Project Area research guidelines, we protected both participant and pedestrian privacy by de-identifying all captured faces using the EgoBlur blurring algorithm [38].

3.2. Dataset Statistics

The final EgoCampus dataset is a large collection of egocentric navigation, totaling approximately 32 hours of multimodal video data (≈ 3.5 million frames). The data was sourced from 82 unique participants, a significant cohort size that provides a diverse set of gaze and movement behaviors. These subjects traversed a set of 25 distinct, predefined paths across a university campus. These paths were specifically chosen to cover outdoor environments on a university campus, with a rich variety of environmental contexts, lighting conditions, and interactions with static and dynamic obstacles. A comparative analysis of the dataset compared to recent egocentric and eye gaze datasets is provided in Tab. 1.

4. Methodology

Given an egocentric video of length T and spatial dimensions H, W . Our goal is to predict the most likely gaze points for each frame $\{f_t \in \mathbb{R}^{3 \times H \times W} | t < T\}$ at time t . The basis of our ECN approach (see Fig. 1) is the assumption that information observed in the past (represented as the video) will influence a person’s future gaze behavior. While videos are very high dimensional, much of the information present is redundant. This leads us to use pretrained video encoder backbones, which greatly reduce the dimensionality of our input while retaining the most useful information. For video backbones, we primarily use X3D [9], but a 3D ResNet [10] is evaluated in Sec. 5.3. An overview of our method is presented in Fig. 4. Through light-weight CNN blocks, we fuse the spatio-temporal features from the video encoder backbones with learned features from a query frame. After fusion, a CNN decoder predicts the final gaze heatmap with the same spatial dimensions of the input, representing the relative likelihood of someone looking at any

| Dataset | Participants | Gaze hours | Pedestrian only | IMU | GPS |
|-------------------------|--------------|------------|-----------------|-----|-----|
| Epic Kitchens [6] | 38 | 0 | ✗ | ✗ | ✓ |
| AND [34] | N/A* | 4 | ✓ | ✓ | ✓ |
| EGTEA Gaze+ [29] | 32 | 28 | ✗ | ✗ | ✗ |
| Ego4D [12] | 80† | 33 | ✗ | ✓ | ✗ |
| GEETUP [42] | 43 | 38 | ✓ | ✓ | ✗ |
| EgoCampus (ours) | 82 | 32 | ✓ | ✓ | ✓ |

Table 1. **A comparative analysis of EgoCampus against other key egocentric datasets.** A comparison of our dataset’s attributes against prominent benchmarks in egocentric vision. The “Pedestrian Only” column specifically denotes datasets that focus on outdoor pedestrian egomotion, as opposed to indoor, task-oriented scenarios (e.g., EGTEA Gaze+, Epic Kitchens). While other datasets like AND and GEETUP also capture outdoor pedestrian trajectories, EgoCampus uniquely integrates all features essential for real-world navigation research: a large-scale participant pool, extensive gaze data, and fully synchronized multimodal data, including rich inertial (IMU) sensors.

* AND [34] does not report a number of participants.

† As reported in [27].

part of the image.

We provide the video encoder backbone with the input video and obtain spatio-temporal features $S \in \mathbb{R}^{N \times f_D}$ where $N = T \times \frac{H}{p} \times \frac{W}{p}$, with video encoder patch size p feature dimensionality f_D . For predicting the gaze of frame f_t , the t -th feature in the time axis of S is fed into ResNeXt blocks [49] to obtain $S' \in \mathbb{R}^{H/4 \times W/4 \times 96}$. To obtain the image features, f_t is fed into ResNeXt blocks to obtain an identically shaped feature map I . S' and I are concatenated along the channel dimension to obtain an encoded gaze map $G \in \mathbb{R}^{H/4 \times W/4 \times 192}$. Then, a learned CNN decoder network upscales the low-res feature map. Finally, the output is blurred, the center prior is added, and a normalization step produces the predicted gaze heatmap.

Models were implemented and trained on a single NVIDIA RTX 3090 GPU in the PyTorch framework. The ADAM optimizer [21] was used with an MSE loss and a learning rate of 0.002. Our final model trained for 10 epochs in approximately 8 hours.

5. Experiments

We first review the evaluation metrics we use for gaze prediction in Sec. 5.1. We also compare EgoCampus-Net (ECN) to existing models from the domains of image saliency, video saliency, and eye gaze prediction in Sec. 5.2. We then present an ablation study on the video feature backbone utilized in the model in section Sec. 5.3 (Excluding ablations, our method is evaluated with a video backbone based on X3D [9]). Finally, we showcase qualitative results and discuss the observed behaviors of the model in Sec. 5.4. We present the results of our model trained on our data,

compared to the performance of existing pretrained models, which we do not train on our data. To demonstrate the need for further research in this area, we show that existing SOTA models do not generalize well enough to have strong performance on our dataset without fine tuning.

For our experiments, we sample the EgoCampus dataset 16 frames at a time, uniformly sampled from a window of 64 frames (≈ 2.1 seconds). Models that utilize temporal information are provided with the full video clip in order to predict gaze in the last frame, while image-based models are only provided with the last frame for prediction. The test/train split follows an approximate 70/30 ratio, where a randomly selected set of 16 paths are reserved for training, and the remaining 9 paths are used for testing. Exact splits will be provided in supplementary material.

5.1. Evaluation Metrics

It is important to distinguish between the broader task of eye gaze prediction and the more specific task of saliency map prediction, as both are relevant to our work. Saliency prediction typically addresses “free-viewing” scenarios, where the goal is to model fixation density across a scene, making it well-suited for evaluation with distribution-based metrics like correlation coefficient (CC), Kullback-Leibler divergence (KLD), and similarity (SIM). In contrast, eye gaze prediction often involves task-specific contexts, such as the navigation-driven behavior captured in EgoCampus, where a person’s attention is directed by their goals rather than just visual conspicuity.

To evaluate the accuracy of predicted saliency maps, we employ two categories of metrics: location-based and distribution-based measures [2]. Location-based metrics, such as AUC-Judd (Area under the ROC curve) and NSS (Normalized Scanpath Saliency), rely on binary fixation maps as ground truth and emphasize how well the model identifies specific salient points. In contrast, distribution-based metrics, such as CC, SIM, and KLD, use continuous grayscale saliency maps to assess the similarity between predicted and ground truth distributions. For all metrics, larger values indicate better alignment, except for KLD, where smaller values reflect greater accuracy.

Area Under Curve (AUC-Judd): AUC-Judd measures how well the predicted saliency map distinguishes between fixated and non-fixated locations using a binary ground truth fixation map. It computes the area under the Receiver Operating Characteristic (ROC) curve. This curve is generated by plotting the True Positive Rate (TPR) (the hit rate, or the percentage of fixations correctly identified as positive) against the False Positive Rate (FPR) (the false alarm rate, or the percentage of non-fixations incorrectly identified as positive) while varying a threshold on the predicted saliency values. Since AUC-Judd summarizes the entire curve, it is

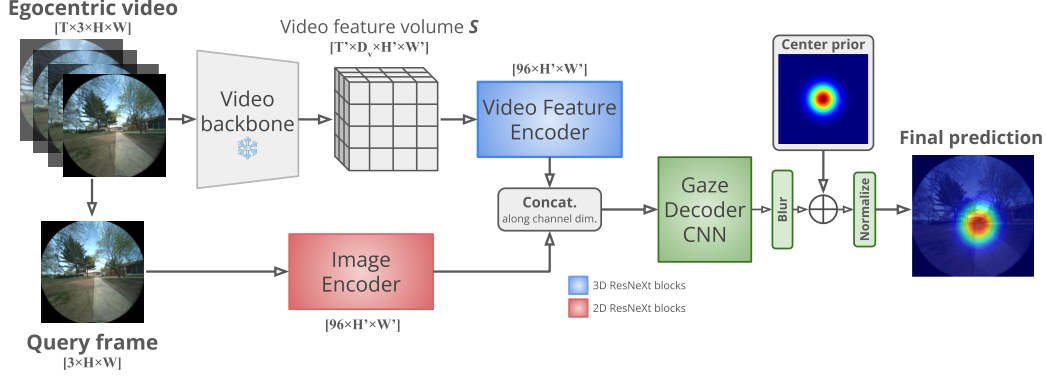


Figure 4. **An overview of the proposed spatio-temporal fusion method.** A pre-trained video feature extractor backbone is used to extract spatio-temporal features that encode information about the input frames. The spatio-temporal features are encoded and upsampled with a ResNet block. In parallel, the query frame is encoded with a separate ResNet block. The image features and spatio-temporal features are concatenated along the feature dimension before being decoded into the final output.

independent of thresholds and provides a robust ranking of predicted saliency at fixated points. Higher values indicate stronger model performance.

$$AUC_{Judd} = \sum_{i=1}^{n-1} \frac{(TPR_i + TPR_{i+1})}{2} \times (FPR_{i+1} - FPR_i) \quad (1)$$

Correlation Coefficient (CC): CC captures the linear correlation between the pixel values of the predicted saliency map (P) and the ground truth distribution (Q). Unlike metrics that use a binary ground truth, CC requires a continuous ground truth map (Q), which is typically created by applying a Gaussian blur to the binary fixation points. This creates a ground truth density map. The metric then treats P and Q as two long vectors of pixel intensities.

$$CC = \frac{\text{cov}(P, Q)}{\sigma(P) \times \sigma(Q)} \quad (2)$$

As shown in the formula, the score is calculated by taking the covariance of P and Q (how their pixel values vary together) and normalizing it by the product of their individual standard deviations (σ), which measure the contrast or “spread” of each map. This assesses whether the spatial patterns co-vary. A high positive value (near 1) implies strong similarity, meaning that bright, high-saliency regions in the prediction P align with high-density regions in the ground truth Q . A score near 0 indicates no linear relationship.

Kullback-Leibler Divergence (KLD): KLD measures the dissimilarity between the predicted and ground truth saliency distributions. To create these distributions, both maps are first converted into probability mass functions (PMFs) where all pixel values sum to 1. The ground truth

distribution (Q) is created by normalizing the binary fixation map by dividing by the total number of fixations. The predicted distribution (P) is created by normalizing the continuous saliency map by dividing by the sum of all its pixel values. KLD then penalizes deviations from the actual human gaze distribution, offering a fine-grained view of prediction errors. ϵ is a small constant added for numerical stability, preventing division by zero where a ground truth fixation $Q(i)$ exists but the prediction $P(i)$ is zero. Lower KLD values (closer to 0) reflect more accurate predictions.

$$\text{KLD}(P \parallel Q) = \sum_i Q(i) \log \left(\frac{Q(i)}{P(i) + \epsilon} \right), \quad (3)$$

Similarity (SIM): SIM quantifies the degree of structural overlap between the predicted and ground truth saliency distributions. To compute this, both the predicted saliency map (P) and the ground truth fixation map (Q) are first normalized into probability mass functions (PMFs), where the sum of all pixel values in each map equals 1. Q is the binary map divided by the count of fixations, and P is the heatmap divided by the sum of all its values.

$$\text{SIM} = \sum_i \min(P(i), Q(i)) \quad (4)$$

The formula then sums the minimum probability value between P and Q at every pixel location i . Conceptually, this calculation measures the intersection area of the two probability distributions. A score of 1 would mean a perfect match in the shape, location, and density of the two distributions. A score of 0 would mean no overlap. This metric rewards predictions that match the overall structure of the ground truth, as it is regardless of absolute intensity, which is removed by the initial normalization step.

Normalized Scanpath Saliency (NSS): NSS evaluates the correspondence between predicted saliency and human fixations. First, it normalizes the entire prediction map. Then, it computes the mean of the saliency values found only at the fixation locations. The entire predicted saliency map (S) is transformed into a standard score (z-score) map, \hat{S} , by subtracting the map’s mean (μ) and dividing by its standard deviation (σ). This gives the normalized map \hat{S} a zero mean and unit variance.

$$\text{NSS} = \frac{1}{N} \sum_{i=1}^N \hat{S}(x_i) \quad (5)$$

As the equation shows, the final score is the average of the normalized \hat{S} values found at the N ground truth fixation locations (x_i). The resulting score is directly interpretable: an NSS of 1.5 means the predicted saliency at fixation points was, on average, 1.5 standard deviations above the map’s mean. A score of 0 indicates performance no better than chance. This metric is highly sensitive to false positives (which raise the map’s mean, μ , thus lowering the score) and strongly rewards spatially precise, high-amplitude predictions at the correct fixation points.

| Model | AUC-J \uparrow | CC \uparrow | KLD \downarrow | SIM \uparrow | NSS \uparrow | # Parameters |
|-------------------|------------------|---------------|------------------|----------------|----------------|--------------|
| Center Prior | 0.925 | 0.423 | 1.347 | 0.403 | 1.511 | - |
| GBVS [13] | 0.912 | 0.483 | 1.812 | 0.577 | 1.988 | 78.9M |
| GazeLLE [29] | 0.976 | 0.823 | 2.063 | 0.712 | 1.831 | 321M |
| ECN (Ours) | 0.987 | 0.806 | 0.459 | 0.665 | 4.029 | 12.8M |

Table 2. Comparison with existing **eye gaze** prediction methods, evaluated on the EgoCampus dataset, with the best results bolded.

| Model | AUC-J \uparrow | CC \uparrow | KLD \downarrow | SIM \uparrow | NSS \uparrow | # Parameters |
|-------------------|------------------|---------------|------------------|----------------|----------------|--------------|
| Center Prior | 0.925 | 0.423 | 1.347 | 0.403 | 1.511 | - |
| CV_MM [33] | 0.963 | 0.512 | 0.392 | 0.508 | 2.836 | 420.5M |
| VistaHL [33] | 0.938 | 0.678 | 2.128 | 0.383 | 2.017 | 187.7M |
| ECN (Ours) | 0.987 | 0.806 | 0.459 | 0.665 | 4.029 | 12.8M |

Table 3. Comparison with existing **video saliency** prediction methods, evaluated on the EgoCampus dataset, with the best results bolded.

5.2. Quantitative Evaluation

ECN, when trained on our data, outperforms the pretrained models consistently in almost every instance (Tabs. 2, 3 and 4). Note that the methods used for comparison are not trained on our dataset, whereas our model is. The strongest comparisons come from CV_MM and VistaHL, which have $\times 39$ and $\times 17$ the number of parameters, respectively. Despite the large size of these models, they do not generalize

| Model | AUC-J \uparrow | CC \uparrow | KLD \downarrow | SIM \uparrow | NSS \uparrow | # Parameters |
|-------------------|------------------|---------------|------------------|----------------|----------------|--------------|
| Center Prior | 0.925 | 0.423 | 1.347 | 0.403 | 1.511 | - |
| DeepGazeIIE [30] | 0.962 | 0.286 | 1.431 | 0.128 | 2.027 | 104M |
| EML-NET [17] | 0.939 | 0.438 | 0.773 | 0.169 | 2.192 | 47.2M |
| SUM [14] | 0.923 | 0.381 | 2.312 | 0.329 | 1.207 | 57.5M |
| TempSAL [1] | 0.904 | 0.468 | 2.812 | 0.356 | 1.513 | 28.6M |
| ECN (Ours) | 0.987 | 0.806 | 0.459 | 0.665 | 4.029 | 12.8M |

Table 4. Comparison with existing **image saliency** prediction methods, evaluated on the EgoCampus dataset, with the best results bolded.

well enough to out perform our smaller model in this domain. It is worth noting that the center prior baseline has competitive results, in relation to the other comparisons. Alongside qualitative results, this indicates that the center bias is strongly present in the egocentric locomotion setting.

5.3. Ablation Study

We perform an ablation study on our method by evaluating model performance with different video feature extractor backbones. We also evaluate the method in the absence of video-image feature fusion altogether, evaluating the impact on temporal information on prediction accuracy. The results of this ablation are shown in Tab. 5.

| Video backbone | AUC-J \uparrow | CC \uparrow | KLD \downarrow | SIM \uparrow | NSS \uparrow | # Parameters |
|-------------------|------------------|---------------|------------------|----------------|----------------|--------------|
| No video features | 0.981 | 0.744 | 0.605 | 0.599 | 3.578 | 6.1M |
| Slow_R50 [10] | 0.986 | 0.799 | 0.458 | 0.663 | 3.895 | 42.5M |
| X3D [9] | 0.987 | 0.806 | 0.459 | 0.665 | 4.029 | 12.8M |

Table 5. Performance of EgoCampusNet (ECN) model with **varying video feature extractor backbones**. Ablation of video features results in notably worse performance, but different backbones attain only marginally different performance. # Parameters denotes the number of parameters in ECN when using the specified backbone.

The inclusion of video backbones in our method is validated by increased performance. This result indicates that some degree of video understanding is beneficial for the gaze prediction task. However, despite a large difference in parameter counts, varying between X3D and 3D ResNet (Slow_R50) has little impact on performance. We find X3D to be preferable for training and inference speed.

5.4. Qualitative Results

Qualitative results of different methods on our dataset is shown in Fig. 5. EML-Net [17] and DeepGazeIIE [30] tend to overestimate the likely gaze area. TempSAL [1] often highlights areas in the sky, despite its lack of visual salience. ECN learns a strong contribution from the center bias, often predicting the center of the image, which tends to be the

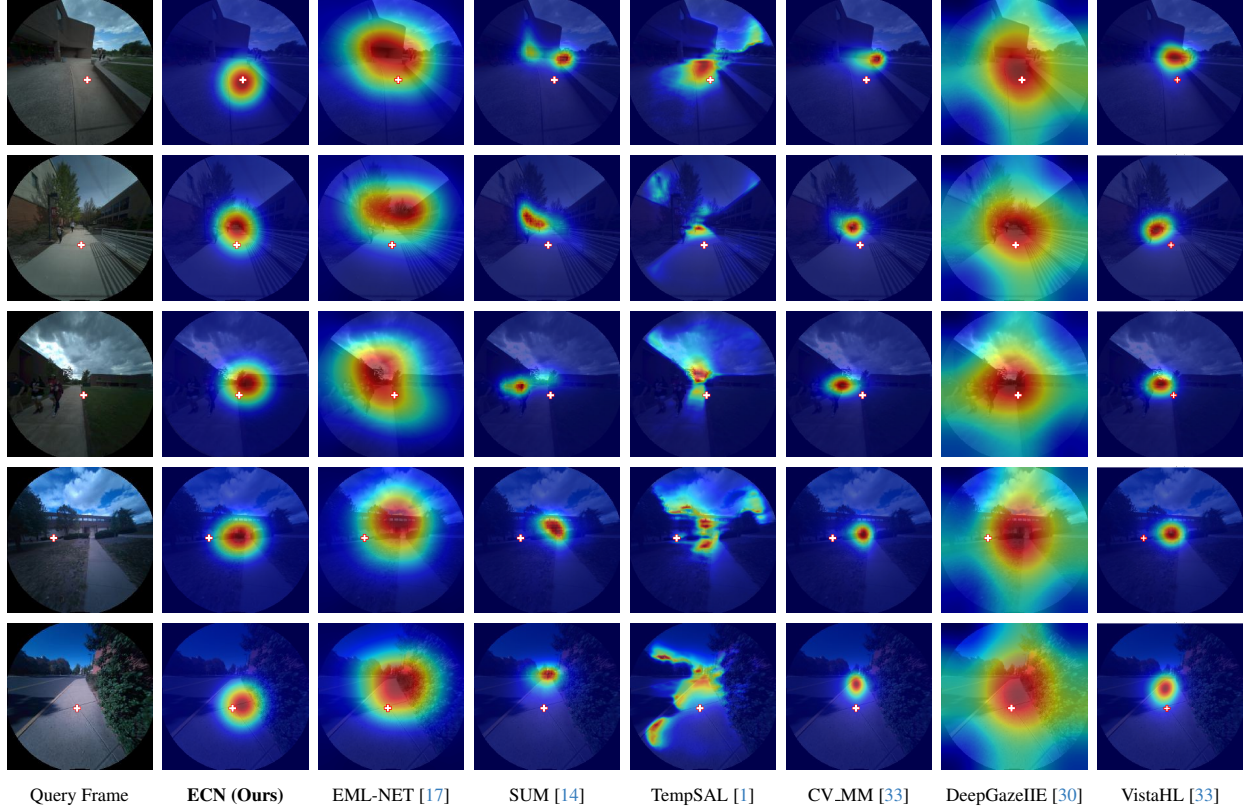


Figure 5. **Qualitative comparison of predicted gaze heat maps on sample frames.** For each scene (row), we show the query frame with the gaze point, the output from our proposed model, and outputs from six comparison methods. Our model consistently produces a more focal heatmap that is more accurately centered on the true gaze point. Note that the white + icon denotes true gaze point in all images.

direction of the subject’s movement during recording. ECN also captures the nuance of task-specific points of interest—namely doors and sidewalks. When the subject walks past other pedestrians, other models often predict that other peoples’ faces is the most likely place to look, but in the setting of egocentric locomotion, this is often not the case.

6. Conclusion

In this work, we introduce EgoCampus, a novel multimodal egocentric dataset designed to facilitate the study of human attention during real-world navigation. By capturing synchronized video, eye gaze, and inertial data from numerous participants traversing shared outdoor routes, EgoCampus provides a unique resource for building and evaluating the next generation of visual attention models. We present EgoCampusNet, which fuses spatio-temporal features from a video encoder backbone with image features learned from the individual query frame. Our experiments demonstrate that this approach sets a strong benchmark for our dataset but, more importantly, exhibits task-dependent adaptations that result in higher performance in egocentric pedestrian video. The findings from this research have sig-

nificant implications for embodied AI and human-robot interaction. The EgoCampus dataset opens avenues for investigating more complex social navigation scenarios, such as group navigation and obstacle avoidance, pushing the frontier of environment-aware attention modeling.

The EgoCampus dataset will be made publicly available and has a **companion dataset** YOPO-Campus [31], where the same campus paths (6 km) were traversed by a tele-operated Clearpath Jackal robot. While YOPO-Campus shows the paths from a robot view, EgoCampus shows the paths from a pedestrian view and capture eye gaze. Together, both datasets provide an important data resource for future studies of navigation in human-robot systems.

Acknowledgments

This work was supported by the NSF-NRT grant: Socially Cognizant Robotics for a Technology Enhanced Society (SOCRATES), No. 2021628 and NSF CNS Reality-Aware Networks No. 1901355. Thank you to Meta for allowing us to use the Project Aria glasses.

References

- [1] Bahar Aydemir, Ludo Hoffstetter, Tong Zhang, Mathieu Salzmann, and Sabine Süsstrunk. Tempsal - uncovering temporal information for deep saliency prediction. In *Proceedings of the IEEE/CVF Conference on Computer Vision and Pattern Recognition (CVPR)*, 2023. 3, 7, 8
- [2] Zoya Bylinskii, Tilke Judd, Aude Oliva, Antonio Torralba, and Frédo Durand. What do different evaluation metrics tell us about saliency models? *IEEE transactions on pattern analysis and machine intelligence*, 41(3):740–757, 2018. 5
- [3] Giuseppe Cartella, Vittorio Cuculo, Alessandro D’Amelio, Marcella Cornia, Giuseppe Boccignone, and Rita Cucchiara. Modeling human gaze behavior with diffusion models for unified scanpath prediction. In *Proceedings of the IEEE/CVF International Conference on Computer Vision*, pages 16206–16216, 2025. 2
- [4] Yupei Chen, Zhibo Yang, Seoyoung Ahn, Dimitris Samaras, Minh Hoai, and Gregory Zelinsky. Coco-search18 fixation dataset for predicting goal-directed attention control. *Scientific reports*, 11(1):8776, 2021. 3
- [5] Maurizio Corbetta and Gordon L Shulman. Control of goal-directed and stimulus-driven attention in the brain. *Nature reviews neuroscience*, 3(3):201–215, 2002. 2
- [6] Dima Damen, Hazel Doughty, Giovanni Maria Farinella, Sanja Fidler, Antonino Furnari, Evangelos Kazakos, Davide Moltisanti, Jonathan Munro, Toby Perrett, Will Price, and Michael Wray. Scaling egocentric vision: The epic-kitchens dataset. In *European Conference on Computer Vision (ECCV)*, 2018. 3, 5
- [7] Jakob Engel, Kiran Somasundaram, Michael Goesele, Albert Sun, Alexander Gamino, Andrew Turner, Arjang Talattof, Arnie Yuan, Bilal Souti, and et. al Brighid Meredith. Project aria: A new tool for egocentric multi-modal ai research, 2023. 2, 3
- [8] Alireza Fathi, Yin Li, and James M Rehg. Learning to recognize daily actions using gaze. In *European Conference on Computer Vision*, pages 314–327. Springer, 2012. 2
- [9] Christoph Feichtenhofer. X3d: Expanding architectures for efficient video recognition, 2020. 4, 5, 7
- [10] Christoph Feichtenhofer, Haoqi Fan, Jitendra Malik, and Kaiming He. Slowfast networks for video recognition. In *Proceedings of the IEEE/CVF international conference on computer vision*, pages 6202–6211, 2019. 4, 7
- [11] Camilo Fosco, Anelise Newman, Pat Sukhum, Yun Bin Zhang, Nanxuan Zhao, Aude Oliva, and Zoya Bylinskii. How much time do you have? modeling multi-duration saliency. In *IEEE/CVF Conference on Computer Vision and Pattern Recognition (CVPR)*, 2020. 3
- [12] Kristen Grauman, Andrew Westbury, Eugene Byrne, Vincent Cartillier, Zachary Chavis, Antonino Furnari, Rohit Girdhar, Jackson Hamburger, Hao Jiang, Devansh Kukreja, et al. Ego4d: Around the world in 3,000 hours of egocentric video. *IEEE Transactions on Pattern Analysis and Machine Intelligence*, pages 1–32, 2024. 1, 3, 5
- [13] Jonathan Harel, Christof Koch, and Pietro Perona. Graph-based visual saliency. *Advances in neural information processing systems*, 19, 2006. 2, 7
- [14] Alireza Hosseini, Amirhossein Kazerooni, Saeed Akhavan, Michael Brudno, and Babak Taati. Sum: Saliency unification through mamba for visual attention modeling. In *Proceedings of the Winter Conference on Applications of Computer Vision (WACV)*, pages 1597–1607, 2025. 2, 7, 8
- [15] Xun Huang, Chengyao Shen, Xavier Boix, and Qi Zhao. Salicon: Reducing the semantic gap in saliency prediction by adapting deep neural networks. In *2015 IEEE International Conference on Computer Vision (ICCV)*, pages 262–270, 2015. 2
- [16] L. Itti, C. Koch, and E. Niebur. A model of saliency-based visual attention for rapid scene analysis. *IEEE Transactions on Pattern Analysis and Machine Intelligence*, 20(11):1254–1259, 1998. 2
- [17] Sen Jia and Neil D.B. Bruce. Eml-net: An expandable multi-layer network for saliency prediction. *Image and Vision Computing*, 95:103887, 2020. 2, 7, 8
- [18] Ming Jiang, Shengsheng Huang, Juanyong Duan, and Qi Zhao. Salicon: Saliency in context. In *Proceedings of the IEEE Conference on Computer Vision and Pattern Recognition (CVPR)*, 2015. 3
- [19] Tilke Judd, Krista Ehinger, Frédo Durand, and Antonio Torralba. Learning to predict where humans look. In *2009 IEEE 12th International Conference on Computer Vision*, pages 2106–2113, 2009. 3
- [20] Petr Kellnhofer, Adria Recasens, Simon Stent, Wojciech Matusik, and Antonio Torralba. Gaze360: Physically unconstrained gaze estimation in the wild. In *Proceedings of the IEEE/CVF International Conference on Computer Vision (ICCV)*, 2019. 3
- [21] Diederik P. Kingma and Jimmy Ba. Adam: A method for stochastic optimization. In *3rd International Conference on Learning Representations, ICLR 2015, San Diego, CA, USA, May 7-9, 2015, Conference Track Proceedings*, 2015. 5
- [22] Chen Kong, James Fort, Aria Kang, Jonathan Wittmer, Simon Green, Tianwei Shen, Yipu Zhao, Cheng Peng, Gustavo Solaira, Andrew Berkovich, Nikhil Raina, Vijay Baiyya, Evgeniy Oleinik, Eric Huang, Fan Zhang, Julian Straub, Mark Schwesinger, Luis Pesqueira, Xiaqing Pan, Jakob Julian Engel, Carl Ren, Mingfei Yan, and Richard Newcombe. Aria gen 2 pilot dataset, 2025. 3
- [23] Eileen Kowler. Eye movements: The past 25 years. *Vision research*, 51(13):1457–1483, 2011. 3
- [24] Kyle Krafka, Aditya Khosla, Petr Kellnhofer, Harini Kannan, Suchendra Bhandarkar, Wojciech Matusik, and Antonio Torralba. Eye tracking for everyone. In *Proceedings of the IEEE Conference on Computer Vision and Pattern Recognition (CVPR)*, 2016. 3
- [25] Prajnaya Kumar, Eshika Khandelwal, Makarand Tapaswi, and Vishnu Sreekumar. Eye vs. ai: Human gaze and model attention in video memorability. *arXiv preprint arXiv:2311.16484*, 2023. 3
- [26] Matthias Kümmerer, Thomas SA Wallis, and Matthias Bethge. Deepgaze ii: Reading fixations from deep features trained on object recognition. *arXiv preprint arXiv:1610.01563*, 2016. 3

- [27] Bolin Lai, Miao Liu, Fiona Ryan, and James M. Rehg. In the eye of transformer: Global–local correlation for egocentric gaze estimation and beyond. *International Journal of Computer Vision*, 132(3):854–871, 2024. 2, 3, 5
- [28] Yin Li, Alireza Fathi, and James M. Rehg. Learning to predict gaze in egocentric video. In *Proceedings of the IEEE International Conference on Computer Vision (ICCV)*, 2013. 2
- [29] Yin Li, Miao Liu, and James M Rehg. In the eye of the beholder: Gaze and actions in first person video. *IEEE transactions on pattern analysis and machine intelligence*, 45(6): 6731–6747, 2021. 3, 5, 7
- [30] Akis Linardos, Matthias Kümmerer, Ori Press, and Matthias Bethge. Deepgaze iie: Calibrated prediction in and out-of-domain for state-of-the-art saliency modeling. In *Proceedings of the IEEE/CVF International Conference on Computer Vision (ICCV)*, pages 12919–12928, 2021. 3, 7, 8
- [31] Ryan Meegan, Adam D’Souza, and Kristin Dana. Yopo-nav: Visual navigation using 3dgs graphs from one-pass videos. *ArXiv*, 2026. 8
- [32] Sounak Mondal, Zhibo Yang, Seoyoung Ahn, Dimitris Samaras, Gregory Zelinsky, and Minh Hoai. Gazeformer: Scalable, effective and fast prediction of goal-directed human attention. In *Proceedings of the IEEE/CVF Conference on Computer Vision and Pattern Recognition*, pages 1441–1450, 2023. 2
- [33] Andrey Moskalenko, Alexey Bryncev, Dmitry Vatolin, Radu Timofte, Gen Zhan, Li Yang, Yunlong Tang, Yiting Liao, Jiongzhai Lin, Baitao Huang, et al. Aim 2024 challenge on video saliency prediction: Methods and results. In *European Conference on Computer Vision*, pages 178–194. Springer, 2024. 3, 7, 8
- [34] Boxiao Pan, Adam W. Harley, C. Karen Liu, and Leonidas J. Guibas. Lookout: Real-world humanoid egocentric navigation, 2025. 3, 5
- [35] Xiaqing Pan, Nicholas Charron, Yongqian Yang, Scott Peters, Thomas Whelan, Chen Kong, Omkar Parkhi, Richard Newcombe, and Yuheng (Carl) Ren. Aria digital twin: A new benchmark dataset for egocentric 3d machine perception. In *Proceedings of the IEEE/CVF International Conference on Computer Vision (ICCV)*, pages 20133–20143, 2023. 3
- [36] Seonwook Park, Emre Aksan, Xucong Zhang, and Otmar Hilliges. Towards end-to-end video-based eye-tracking. In *European conference on computer vision*, pages 747–763. Springer, 2020. 3
- [37] Toby Perrett, Ahmad Darkhalil, Saptarshi Sinha, Omar Emara, Sam Pollard, Kranti Parida, Kaiting Liu, Prajwal Gatti, Siddhant Bansal, Kevin Flanagan, Jacob Chalk, Zhi-fan Zhu, Rhodri Guerrier, Fahd Abdelazim, Bin Zhu, Davide Moltisanti, Michael Wray, Hazel Doughty, and Dima Damen. Hd-epic: A highly-detailed egocentric video dataset. In *Proceedings of the IEEE/CVF Conference on Computer Vision and Pattern Recognition (CVPR)*, 2025. 3
- [38] Nikhil Raina, Guruprasad Somasundaram, Kang Zheng, Sagar Miglani, Steve Saarinen, Jeff Meissner, Mark Schwesinger, Luis Pesqueira, Ishita Prasad, Edward Miller, et al. Egoblur: Responsible innovation in aria. *arXiv preprint arXiv:2308.13093*, 2023. 4
- [39] Adria Recasens, Aditya Khosla, Carl Vondrick, and Antonio Torralba. Where are they looking? *Advances in neural information processing systems*, 28, 2015. 3
- [40] Hyun Soo Park and Jianbo Shi. Social saliency prediction. In *Proceedings of the IEEE Conference on Computer Vision and Pattern Recognition (CVPR)*, 2015. 2
- [41] Sanket Kumar Thakur, CIGDEM BEYAN, Pietro Morerio, and Alessio Del Bue. Predicting gaze from egocentric social interaction videos and imu data. In *Proceedings of the 2021 International Conference on Multimodal Interaction*, page 717–722, New York, NY, USA, 2021. Association for Computing Machinery. 2
- [42] Matteo Valsecchi, Arash Akbarinia, and Karl Gegenfurtner. Introducing geetup a large database of mobile eye tracking in a urban environment. *Journal of Eye Movement Research*, 12(7), 2019. 5
- [43] Matteo Valsecchi, Arash Akbarinia, Raquel Gil-Rodriguez, and Karl R. Gegenfurtner. Pedestrians egocentric vision: Individual and collective analysis. In *ACM Symposium on Eye Tracking Research and Applications*, New York, NY, USA, 2020. Association for Computing Machinery. 3
- [44] Kang Wang, Hui Su, and Qiang Ji. Neuro-inspired eye tracking with eye movement dynamics. In *Proceedings of the IEEE/CVF conference on computer vision and pattern recognition*, pages 9831–9840, 2019. 3
- [45] Wenguan Wang, Jianbing Shen, Fang Guo, Ming-Ming Cheng, and Ali Borji. Revisiting video saliency: A large-scale benchmark and a new model. In *Proceedings of the IEEE Conference on computer vision and pattern recognition*, pages 4894–4903, 2018. 3
- [46] Xin Wang, Taein Kwon, Mahdi Rad, Bowen Pan, Ishani Chakraborty, Sean Andrist, Dan Bohus, Ashley Feniello, Bugra Tekin, Felipe Vieira Frujeri, Neel Joshi, and Marc Pollefeys. Holoassist: an egocentric human interaction dataset for interactive ai assistants in the real world, 2023. 3
- [47] Zirui Wang, Wenjing Bian, Xinghui Li, Yifu Tao, Jianeng Wang, Maurice Fallon, and Victor Adrian Prisacariu. Seeing in the dark: Benchmarking egocentric 3d vision with the oxford day-and-night dataset, 2025. 3
- [48] Jeremy M Wolfe and Todd S Horowitz. Five factors that guide attention in visual search. *Nature human behaviour*, 1(3):0058, 2017. 2
- [49] Saining Xie, Ross Girshick, Piotr Dollár, Zhuowen Tu, and Kaiming He. Aggregated residual transformations for deep neural networks. *arXiv preprint arXiv:1611.05431*, 2016. 5
- [50] Kentaro Yamada, Yusuke Sugano, Takahiro Okabe, Yoichi Sato, Akihiro Sugimoto, and Kazuo Hiraki. Can saliency map models predict human egocentric visual attention? In *Computer Vision – ACCV 2010 Workshops*, pages 420–429, Berlin, Heidelberg, 2011. Springer Berlin Heidelberg. 3
- [51] Zhibo Yang, Sounak Mondal, Seoyoung Ahn, Gregory Zelinsky, Minh Hoai, and Dimitris Samaras. Target-absent human attention. In *European Conference on Computer Vision*, pages 52–68. Springer, 2022. 2